Langmuir

Article

pubs.acs.org/Langmuir

Au–Silica Nanowire Nanohybrid as a Hyperthermia Agent for Photothermal Therapy in the Near-Infrared Region

Jiao Chen,[†] Xuefeng Li,[‡] Xu Wu,[†] Joshua T. Pierce,[†] Nenny Fahruddin,[†] Min Wu,*[,‡] and Julia Xiaojun Zhao*[,†]

[†]Department of Chemistry and [‡]Department of Biochemistry and Molecular Biology, University of North Dakota, Grand Forks, North Dakota 58202, United States

ABSTRACT: Nanomaterial-based photothermal therapy has shown great potential for efficient cancer treatment. Here, we report a new hyperthermia agent, Au–silica nanowire nanohybrid (Au-SiNW nanohybrid) with tunable optical properties, for photothermal therapy. The unique feature of the synthetic method is no need of surface modification of SiNWs for the direct deposition of Au seeds, which can avoid complicated synthetic procedures and improve the reproducibility. The Au-SiNW nanohybrid can generate significant amount of heat upon irradiation in the near-infrared (NIR) region for inducing thermal cell death. Moreover, compared to reported hyperthermia nanomaterials, the new nanohybrid requires a much lower laser irradiation density of 0.3 W/cm^2 for destroying cancer cells. A549 lung cancer cells were used for *in vitro* photothermal study. The nanohybrid showed excellent *in vitro* biocompatibility by using a 96-nonradioactive-cell proliferation assay. Even at a high concentration of 0.500 mg/mL nanohybrid, over 80% cells were alive. In contrast, almost all the cells were killed when NIR irradiation was applied at a concentration of 0.100 mg/mL nanohybrid. The Au-SiNW nanohybrid may become a promising hyperthermia agent.

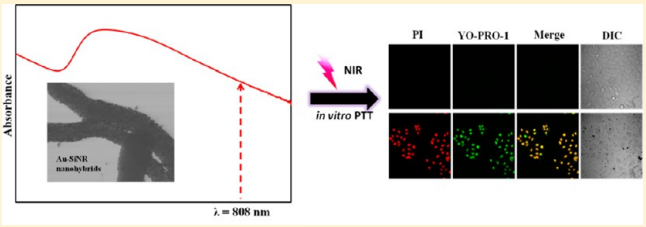

1. INTRODUCTION

Core–shell nanohybrids made from a metal shell possessed tunable optical properties.[1−4] The most notable optical feature of such nanohybrids is the surface plasmon resonance absorption. Based on the core dimensions and the shell thicknesses, their plasmon resonances can be obtained continuously from ultraviolet to infrared regions of the electromagnetic spectrum, including the near-infrared (NIR) region.[5,6] In the NIR region, light transmission in tissues is much higher than that in the UV–vis region due to low light scattering and absorption from intrinsic chromophores. This resulted in low-energy absorption of NIR light by normal tissues and thus limited damage to normal biological tissues while selectively killing cancer cells based on specific targeting of cancer cells using recognition reagents on the surface of nanohybrids.[7−9] Among various metal shells, gold nanoshells are of special interest due to their inertness in biological medium, good biocompatibility, and easy bioconjugation.[10−15] Therefore, gold nanoshells have attracted noticeable attention in a broad range of applications, including optical communications, biological systems for medical imaging, diagnostic and therapeutic applications, etc.[16−19]

A number of materials have been used for making a core of core–shell nanohybrids.[20−23] Recently, gold shells with various shapes of silica cores have been successfully constructed for Raman and fluorescence signal enhancing and drug delivery.[2,24−28] Silica nanomaterials have shown great promise in various fields due to their unique physical and chemical stability, large surface area, and well-established surface modification.[29−32] Moreover, the gold shell–silica core nanohybrids with a strong NIR absorption could convert photo energy into cytotoxic heat upon NIR laser irradiation. Thus, gold shell–silica core nanohybrids have been considered as hyperthermia agents for photothermal therapy (PTT).[14] However, most of these photothermolysis studies require high laser power irradiation to destroy cancer cells. A common range of this power, 1.5–48.6 W/cm^2,[33−36] is higher than the maximal permissible exposure (MPE) of skin per ANSI (American National Standard for Safe Use of Lasers) regulation (e.g., 0.4 W/cm^2 at 850 nm).[37] Therefore, it is highly needed to design more efficient and safer photothermal materials.

Silica nanowires (SiNWs) are relatively new silica nanomaterials and have attracted great attention due to their unique physical and chemical stability and efficient photoluminescence emission.[38,39] Meanwhile, the SiNWs have stimulated considerable interests in making biological and environmental sensing devices owing to their large surface area, high loading capacity for large molecules, excellent reservoir characteristics, and the well-established protocols for surface modification of silica with bioselective coatings.[40,41] For example, Ramgir et al. applied SiNW as an effective template for the real-time detection of potential lung cancer biomarkers (interleuking-10). Because of the high surface-to-volume ratio, the SiNWs greatly enhanced the loading of a specific capture antibody toward a particular

Received: October 31, 2013
Revised: July 13, 2014
Published: July 16, 2014

   dx.doi.org/10.1021/la5020434 | *Langmuir* 2014, 30, 9514–9523

cancer antigen, resulting in a low detection limit down to 1 fg/mL in ideal pure solution and 1 pg/mL in clinically relevant samples.[42]

In this work, SiNW was used as a core to make the core−shell nanohybrid. With the modification of numerous gold nanoparticles (AuNPs) on the surface of SiNWs, we found that this new type of nanohybrid material had strong absorption in the NIR region and can efficiently generate heat under NIR irradiation. Remarkably, a much lower laser power irradiation, 0.30 W/cm^2, lower than the MPE of skin, was enough for photodestruction of cancer cells *in vitro* by applying the Au-SiNW nanohybrids. The optimal conditions of the Au-SiNW nanohybrids as hyperthermia agents for photothermal cancer therapy were studied. Our results demonstrated that this new nanohybrid could be a potential candidate for new photothermal materials.

2. EXPERIMENTAL SECTION

2.1. Materials and Instrumentation. Tetraethyl orthosilicate (TEOS, 98%) was purchased from Acros Organics. Sodium citrate (Na_3Ct), gold(III) chloride trihydrate ($HAuCl_4{\cdot}3H_2O$, 99.9+%), hydroxylamine hydrochloride (98%, ACS grade), tris(bipyridine)-ruthenium(II) chloride ($Ru(bpy)_3^{2+}$, and sodium borohydride ($NaBH_4$, >98%) were purchased from Sigma-Aldrich Inc. Ammonium hydroxide (NH_4OH, 28.0%−30.0%), potassium carbonate ($K_2CO_3{\cdot}1.5H_2O$, ACS grade), dimethyl sulfoxide (DMSO), (4-(2-hydroxyethyl)-1-piperazineethanesulfonic acid (HEPES), and ethanol (95%) were obtained from Fisher Scientific Co. Polyvinylpyrrolidone molecule (PVP, average molecular weight M_n = 40 000) and 1-pentanol (99+%, ACS grade) were purchased from Alfa Aesar. Sodium dodecyl sulface (SDS) was purchased from BioRAD. Dulbecco's modified eagle medium (DMEM) was obtained from Thermo. Human lung epithelial cells (A549 cells) were obtained from American Tissue Culture Collection (ATCC). A 96-nonradioactive-cell proliferation assay (MTT) kit was purchased from Promega. A Vybrant apoptosis assay kit was obtained from Molecular Probes. Deionized water with resistivity of 18.2 MΩ·cm was used in all experiments.

A Hitachi SU8010 field emission scanning electron microscope (SEM) was used to take images of the developed nanohybrids. The elemental analysis of the nanohybrids was achieved by performing energy-dispersive X-ray spectroscopy (EDS) measurements using an Oxford X-Max EDS that is attached to the Hitachi SU8010 field emission SEM. A Shimadzu UV−vis spectrophotometer was used to measure sample absorbance. The size of Au seed was measured using a Zetasizer (Marlwen, model of Nano-ZS). A BWF1 series fiber-coupled diode laser system (750 mW at 808 nm) from B&W TEK Inc. was used for photothermal effect study. A SK-1250MC electronic thermometer was purchased from Sato Keiryoki MFG. CO., Ltd.

2.2. Synthesis of Silica Nanowires (SiNWs). An efficient approach to synthesize SiNWs has been developed in our lab. In a typical synthetic process, 3.00 g of PVP was completely dissolved in 30.00 mL of 1-pentanol under the sonication of 20 min. After mixing the PVP with 1-pentanol, a 3.00 mL aliquot of 95% ethanol, 0.84 mL of H_2O, 0.20 mL of 0.17 M Na_3Ct, 0.30 mL of NH_4OH, and 0.30 mL of TEOS were added in succession. The mixed solution was well shaken. The reaction was allowed to proceed overnight at room temperature. The synthesized SiNWs were centrifuged at the speed of 6500 rpm for 30 min and then washed three times by ethanol. Finally, the SiNWs were dissolved in water to prepare a 10.00 mg/mL SiNWs stock solution. For the synthesis of $Ru(bpy)_3^{2+}$-doped SiNWs, the addition of 0.84 mL of H_2O was replaced with 0.84 mL of 0.001 M $Ru(bpy)_3^{2+}$ and then followed the same procedures.

2.3. Preparation of Au Seeds. The gold layer growing method has been well studied in our group.[28] Before growing the gold layer on the surface of SiNWs, Au seeds were synthesized based on a literature method.[43] In a typical Au seed synthesis, 4.00 mL of 1.00% $HAuCl_4$ solution was added into 100.00 mL of water in an ice bath, followed the addition of 0.50 mL of 0.20 M K_2CO_3. The solution was stirred for 10 min until the color turned from bright yellow to colorless (or light yellow). A 5.00 mL aliquot of 0.50 mg/mL $NaBH_4$ solution was then slowly added to the above solution. The formation of reddish solution indicated the successful synthesis of Au seeds. The prepared Au seeds were kept in a refrigerator at 4.0 °C for future use.

2.4. Gold Layer Growth. A 1.00 mL aliquot of 10.00 mg/mL SiNW solution was dropwise added into 40.00 mL of Au seeds and allowed to react for 10 min under vigorous stirring. Surplus Au seeds were removed by centrifugation at a speed of 6500 rpm for 10 min, and then the supernatant was carefully removed. The purplish red precipitate was Au seed-modified SiNWs and was resuspended into 10.00 mL of water. The gold growth solution consisted of 2.00 mL (or 0.50, 1.00, or 4.00 mL) of 1.00% $HAuCl_4$ and 0.025 g of K_2CO_3 in 90.00 mL of water. The growth solution was vigorously stirred until it turned to light yellow or colorless. A 10.00 mL aliquot of presynthesized Au seed-modified SiNWs was added into the growth solution, followed by the addition of 1.00 mL of 0.50 M hydroxylamine hydrochloride. Then, 1.00 g of PVP was added into the above solution to stabilize the nanohybrids. After an overnight stirring, the solution was centrifuged at a speed of 6500 rpm for 15 min and washed three times by ethanol.

2.5. Au Seed Coating on Calcination-Treated SiNWs. The SiNWs synthesized from section 2.2 were calcinated at 400 °C for 4 h to move the PVP molecules. The calcination-treated SiNWs were then dissolved in water to prepare a concentration of 10 mg/mL solution. A 1.00 mL aliquot of 10.00 mg/mL calcination-treated SiNW solution was dropwise added into 40.00 mL of Au seeds and allowed to react for 10 min under vigorous stirring. The solution was then centrifuged at a speed of 6500 rpm for 10 min, and the supernatant was removed.

2.6. Cell Proliferation Assay for Studying Cytotoxicity of the Au-SiNW Nanohybrids. The cytotoxicity of the Au-SiNW nanohybrids was investigated using (3-(4,5-dimethylthiazol-2-yl)-2,5-diphenyltetrazolium bromide (MTT, a cell proliferation assay).[44] Three different cancer cells, including human alveolar epithelial A549, SW620, and KW12C cells, were cultured onto a 96-well plate at 37 °C for 24 h. Then, each well was added 10.00 μL of MTT reagent with a final concentration of 1.00 μg/mL. The cells were further incubated at 37 °C for 4 h until the purple-color developed. Afterward, 100.00 μL of stop solution (10% DMSO, 10% SDS in 50 mM HEPES buffer) was added into each well, and the cells were continuously incubated overnight at 37 °C. The absorbance of each well was recorded at 560 nm to determine the cell proliferation rate.

2.7. Vybrant Apoptosis Assay. Cell apoptosis and necrosis were detected using the Vybrant apoptosis assay. A549 cells were precultured in a DMEM culture medium overnight, and the final cell number was ∼1 × 10^5/well. Then, a final concentration of Au-SiNW nanohybrids varying from 0.100, 0.050, 0.025 to 0.010 mg/mL was obtained in each well of the plate. The cells were incubated at 4 °C for 30 min and then at 37 °C for 2 h. Next, the cells were treated with an 808 nm laser irradiation for 20 min. The cells were washed three times using a fresh cell culture medium and then treated with the fluorescence probe, propidium iodide (PI) and YO-PRO-1 dyes (Vybrant apoptosis assay kit), for 10 min.[45] The cells were observed immediately under a Zeiss confocal fluorescence microscope. The population separated into three groups: live cells with no fluorescence signals, apoptotic cells with high green fluorescence, and necrotic cells with red fluorescence.

3. RESULTS AND DISCUSSION

3.1. Synthesis of Au-SiNW Nanohybrids. *3.1.1. Au Seed Modification.* We first developed a relatively simple method to coat a gold layer on a silica matrix to synthesize the Au-SiNW nanohybrids. The gold layer decoration on the surface of SiNWs was accomplished through a two-stage deposition process. The first step was the seed deposition, and the second was the seeded growth. The unique feature of this method was to directly deposit Au seeds onto the surface of SiNWs without any surface modification in the seed deposition step. Surface

dx.doi.org/10.1021/la5020434 | Langmuir 2014, 30, 9514−9523

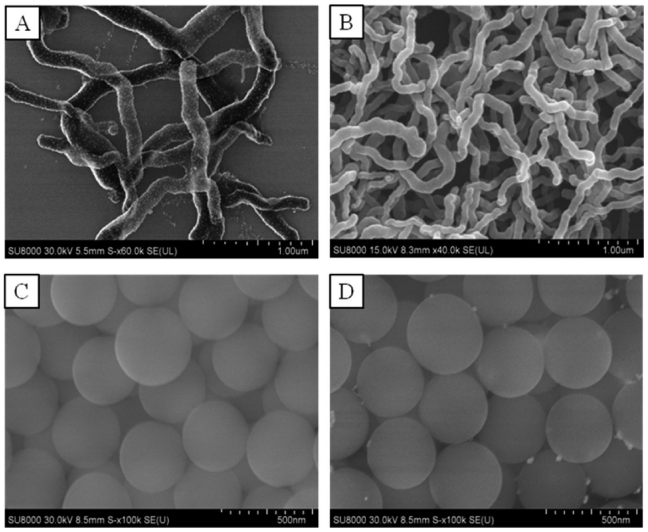

Figure 1. SEM image of (A) SiNWs coated with Au seeds, (B) pure SiNWs, (C) pure silica nanoparticles, and (D) silica nanoparticles coated with few Au seeds due to no PVP used in the sysnthesis.

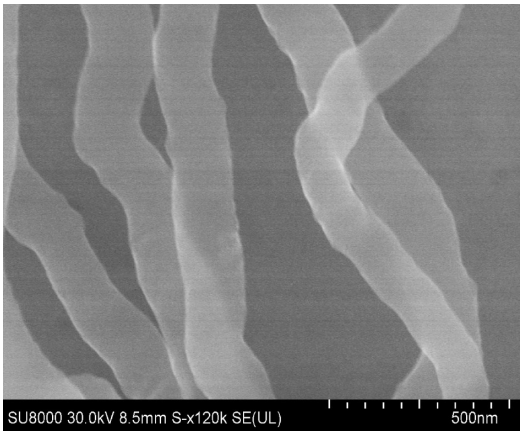

Figure 2. SEM image of calcination-treated SiNWs after stirring with Au seeds.

modification in the process of Au-seed deposition was highly required in most published methods, which constituted complicated synthetic procedures and low reproducibility.[37,38] This step was completely eliminated in our method. The diameter of synthesized Au seeds was measured to be 9.7 ± 1.6 nm using a particle size analyzer. The seed deposition was obtained by simply mixing the Au seeds and the SiNW solution for 10 min and an evenly deposited Au seed layer formed on the surface of the SiNWs (Figure 1A).

The mechanism of the Au seed direct deposition on the SiNWs was studied. The presence of PVP on the SiNWs was a key factor. As described in section 2.2, PVP was added during the synthesis of SiNWs as a surfactant and stabilizer to form the PVP−water droplets in the microemulsion. The hydrolysis and polymerization of TEOS occurred in the interface of PVP−water droplets and oil phase. With continuous reaction, the PVP−water droplet moved to one end and the silica continued to grow along this direction and resulted in an ultralong SiNW (Figure 1B). Although a few times of washing were employed after the synthesis of SiNWs, the PVP was not completely washed away. As well studied, PVP was adsorbed to a broad range of materials including metals (e.g., gold, silver, and iron), metal oxides, silica, etc.[46,47] Thus, the remaining trace PVP used in the synthesis of SiNWs provided the Au seeds with an easy deposition on the SiNW surface.

Two experiments were conducted to confirm the PVP function on this Au seed direct deposition. In the first experiment, we compared our SiNWs with the pure silica nanoparticles that were synthesized with a similar procedure but without the addition of PVP (Figure 1C). When mixing the silica nanoparticles with the Au seeds, few or no Au seeds were decorated on the surface of silica nanoparticles (Figure 1D), showing the crucial role of PVP. The Au seed-decorated SiNWs were then used to nucleate the growth of a gold layer. With the addition of a reducing reagent, hydroxylamine hydrochloride, the Au seeds grew to form a uniform Au layer in the presence of $HAuCl_4$.

In the second experiment, the synthesized SiNWs were treated in a calcination process at 400 °C for 4 h. It has been well-studied that PVP molecules can be removed at high temperature. The calcination-treated SiNWs were then stirring with Au seeds (as described in section 2.5). As shown in Figure 2, no Au seeds were coated on the surface of SiNWs due to the absence of PVP. Both of these two experiments prove the importance of PVP on the deposition of Au seeds on the SiNW surface.

3.1.2. Tune the Plasmon Resonance Band of the Nanohybrid to the NIR Region. We were able to tune the plasmon resonance band of the nanohybrid to the NIR region by systematically increase the thickness of the AuNP layer on the SiNWs. When the amount of $HAuCl_4$ in the Au growth solution increased, the size of AuNPs increased, resulting in different thickness of the AuNP layer on the SiNWs. Figure 3A−D shows the SEM images of SiNWs modified with various sized AuNPs. The size of AuNPs on the surface of SiNWs was statistically measured based on over 200 AuNPs. The result was shown in Figure 3E. When 4.0 mL of 1% $HAuCl_4$ was used in the Au growth solution, the size of the AuNP increased to 57.3 ± 16.9 nm. The morphology of AuNPs on the surface of SiNWs became more irregular shape rather than a spherical shape with the increasing of $HAuCl_4$ amount. To further identify the formation of AuNP layer, the resultant nanohybrids were analyzed using the SEM-EDS elemental analysis. A representative EDS spectrum was presented in Figure 3F. As expected, Au peaks were observed in the spectrum confirming the existence of gold element. Apart from Au signals, the spectrum also showed Si and O signals (from SiNWs) and Cu signal (from the copper grid).

The plasmon resonance band of the nanohybrid was tuned to the NIR region when the AuNP size increased to certain value (Figure 4). The freshly prepared Au seeds showed a peak around 514 nm (Figure 4a) which is consistent with the literature.[48] Upon the attachment of Au seeds on the surface of SiNWs before the addition of growth solution, the plasmon band appeared at 520 nm (Figure 4b), which was slightly red-shifted compared to that of free Au seeds (514 nm). The absorption peak of Au-SiNW nanohybrids increased with the size changes of AuNPs on the surface of SiNWs (Figure 4c−f). With a thicker gold layer, the absorption peak red-shifted toward the NIR region and the peak shape became broader. The broad absorption in the NIR region suggested that the Au-SiNW nanohybrids would be suitable for photothermal therapy. In the NIR region tissues and biological samples have the minimum light absorption, and thus the irradiation has low influence on normal cells. However, pure SiNWs showed little

dx.doi.org/10.1021/la5020434 | *Langmuir* 2014, 30, 9514−9523

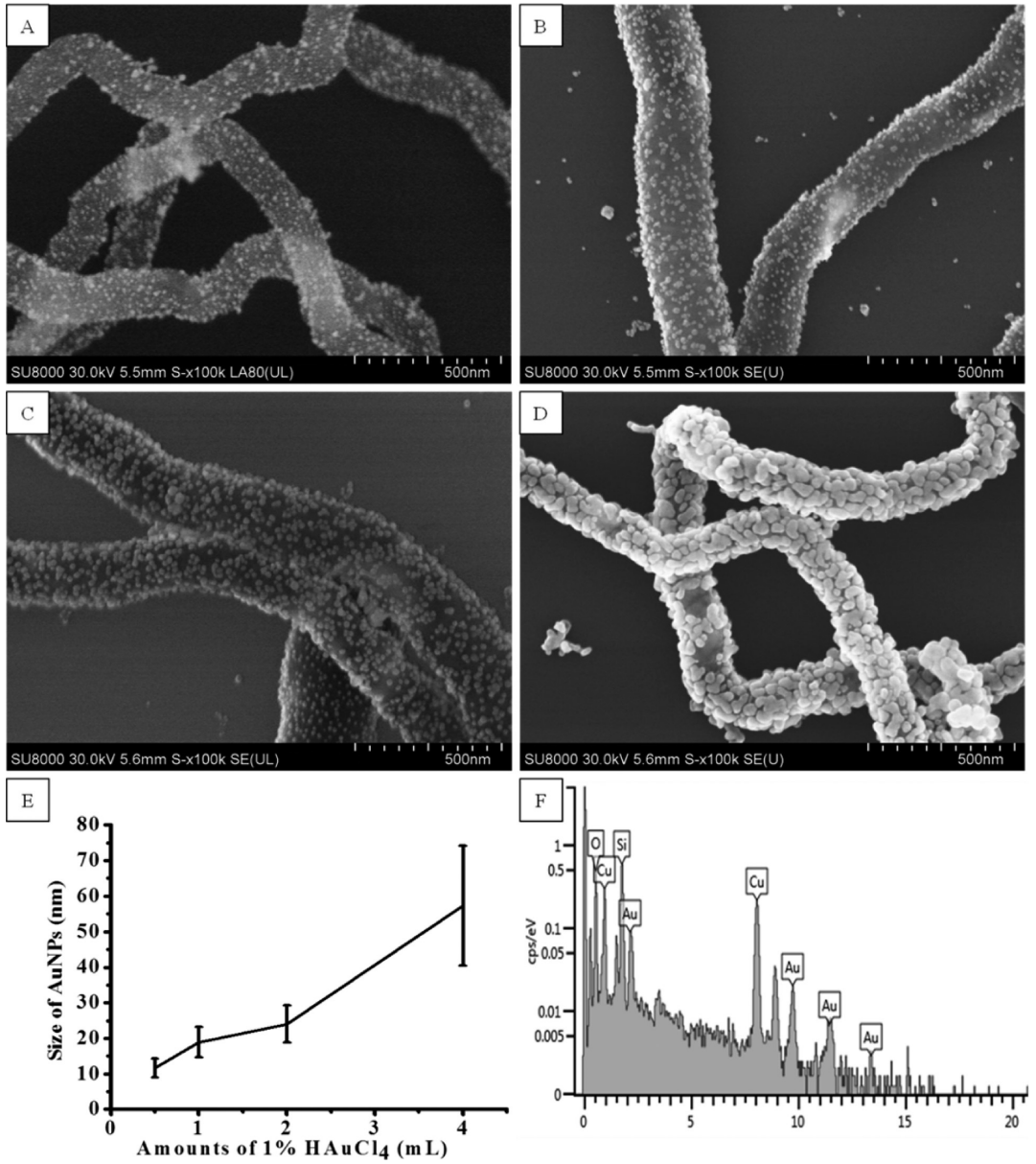

Figure 3. Au-SiNW nanohybrids. (A–D) SEM images of different thicknesses Au layer on SiNW obtained by adding 0.50 (A), 1.00 (B), 2.00 (C), and 4.00 mL (D) of 1.00% $HAuCl_4$ in the gold growth solution. (E) Statistical measurement of the AuNP size. (F) Representative EDS spectrum obtained from the Au-SiNW nanohybrids.

or no NIR absorption (Figure 4g). Although the sample with the thickest gold layer (57.3 ± 16.9 nm) had the highest absorption at 808 nm (Figure 4b), a large number of free AuNPs were obtained besides the Au-SiNW nanohybrids. Therefore, the Au-SiNW nanohybrids used in the following work were synthesized by adding 2.00 mL of 1.00% $HAuCl_4$ to form a gold layer thickness of 24.0 ± 5.2 nm. Moreover, the Au-SiNW nanohybrids showed excellent stability. After storing over one year, the nanohybrids still showed strong NIR absorption which is comparable to the original intensity and well-dispensability (Figure 5).

3.2. Concentration Effect of Au-SiNW Nanohybrids on Plasmon Resonance. The concentration of nanomaterials usually affects their plasmon resonance absorption intensity. Thus, we first investigated light absorption capabilities of the nanohybrids under various concentrations. The spectra shown in Figure 6A indicated that the concentration dependent nature of the nanohybrids. As the concentration increased from 0.00625 to 0.200 mg/mL, the absorbance at 808 nm raised from 0.0533 to 1.3066. It gave a good linear correlation (R^2 = 0.9983) between the absorbance at 808 nm and the concentration of Au-SiNW nanohybrids (Figure 6B). Overall in the NIR region the nanohybrids exhibited strong optical absorption even at low concentrations. As a comparison, we tested pure absorption ability of SiNWs. Their absorption in the NIR region was much weaker (Figure 6C). For example, the absorbance of Au-SiNW nanohybrids reached 0.67 at a concentration of 0.100 mg/mL while only 0.03 for pure SiNWs at the same concentration.

3.3. Photothermal Capability of the Nanohybrids. Because of their high absorption in the NIR region, the Au-SiNW nanohybrid aqueous solution was irradiated with an 808 nm NIR laser at a power density of 0.30 W/cm^2 to study its heat releasing. Four controls were used including water, cell

dx.doi.org/10.1021/la5020434 | *Langmuir* 2014, 30, 9514–9523

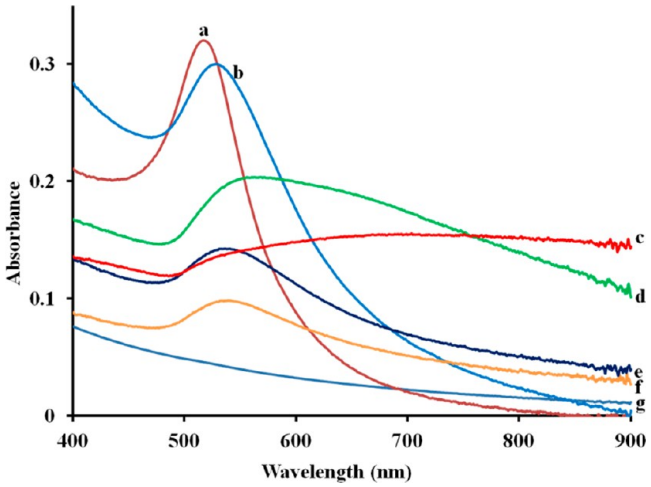

Figure 4. UV−vis spectra of free Au seeds (a), Au-seed coated on SiNWs (b), Au-SiNW nanohybrids by adding 4.00 (c), 2.00 (d), 1.00 (e), and 0.50 mL of 1.00% $HAuCl_4$ (f), and pure SiNWs (g).

medium, pure AuNPs, and pure SiNWs. As shown in Figure 7, no obvious temperature increase was observed for these four controls, indicating a low degree of temperature elevation. In contrast, the Au-SiNW nanohybrids showed a rapid rise in temperature upon exposure to the laser after a short time period of 10 min and reached a plateau after 20 min of irradiation. A higher concentration of Au-SiNW nanohybrids displayed a sharper temperature increase. Moreover, the photothermal effect was also studied by using gold coated on silica nanoparticles (Au-SiNP nanohybrids) to compare the temperature increasing ability. From the obtained results, a higher temperature increasing was achieved when Au-SiNW nanohybrids were used. For example, the temperature can increase to 38.3 and 43.7 °C in the presence of 0.05 and 0.1 mg/mL of Au-SiNW nanohybrids, respectively but only increased to 36.8 and 42.4 °C when the two same concentrations of Au-SiNP nanohybrids were used (data not shown here). These data indicated that the Au-SiNW nanohybrids can act as an efficient photothermal mediator.

3.4. Biocompatibility of the Au-SiNW Nanohybrids. The biocompatibility of the nanohybrids to living systems was examined prior to applying the nanohybrids to *in vitro* phototheramal therapy. A cell proliferation assay (MTT assay) that can detect cellular toxicity was performed to carry the biocompatible evaluation. Because of the presence of PVP in the nanohybrids, we first studied the toxicity of PVP to A549 cancer cells. Different concentrations of PVP solution ranging from 0, 0.5, 1.0, 2.0, 5.0, to 10.0% were studied (Figure 8). Even at high concentrations (5.0 and 10.0%), the cell viability were 84% and 77%, respectively, indicating a good biocompatibility of PVP.

We then studied the biocompatibility of this novel nanohybrid with other three cancer cells, including A549 cells, SW620, and KW12C. Take A549 cells as the example. Different concentrations of the nanohybrids, from 0, 0.010, 0.025, 0.050, 0.075, 0.100, 0.250 to 0.500 mg/mL, were added to A549 cells in a 96-well plate and incubated for 24 h at 37 °C. After this time period, the effect on cell viability was measured as shown in Figure 9. The cell viability decreased as the concentration of Au-SiNW nanohybrids gradually increased from 0.010 to 0.500 mg/mL, showing a concentration-dependent nanotoxicity trend. For example, at a low nanocomposite concentration ($\leq$ 0.100 mg/mL), Au-SiNW nanohybrids had no discernible cell cytotoxicity according to the Student *t*-test ($p > 0.05$). The cell viability was decreased to 80% compared to the untreated control group when high concentrations, 0.250 and 0.500 mg/mL, of Au-SiNW nanohybrids were used.

It showed similar trends in the other two cancer cells, including KW12C and SW620 (Figure 10). As the toxicity observed in these assay was not dramatic, these results demonstrated that the excellent biocompatibility of Au-SiNW nanohybrids would be promising.

3.5. *In Vitro* Photothermal Therapy Application of the Nanohybrids. An important feature of the Au-SiNW nanohybrids is the NIR-induced thermal effect. As demonstrated in section 3.3, the Au-SiNW nanohybrids irradiated by NIR laser clearly elevated the temperature of the solution. This type of nanocomposite could absorb NIR irradiation and then converted the absorbed energy into heat and generate localized hyperthermia. This unique property brought a potential application of the nanohybrids to destroy cancer cells by NIR irradiation on a localized tumor area. To test this potential, we conducted an *in vitro* application of Au-SiNW nanohybrids for photothermal therapy. The Vybrant assay that can distinguish apoptosis and necrosis was used to investigate the PTT effects since apoptosis is considered to be preferred responses among different mechanisms of inducing tumor cell death.[49] Two dyes, the green fluorescent YO-PRO-1 and red fluorescent propidium

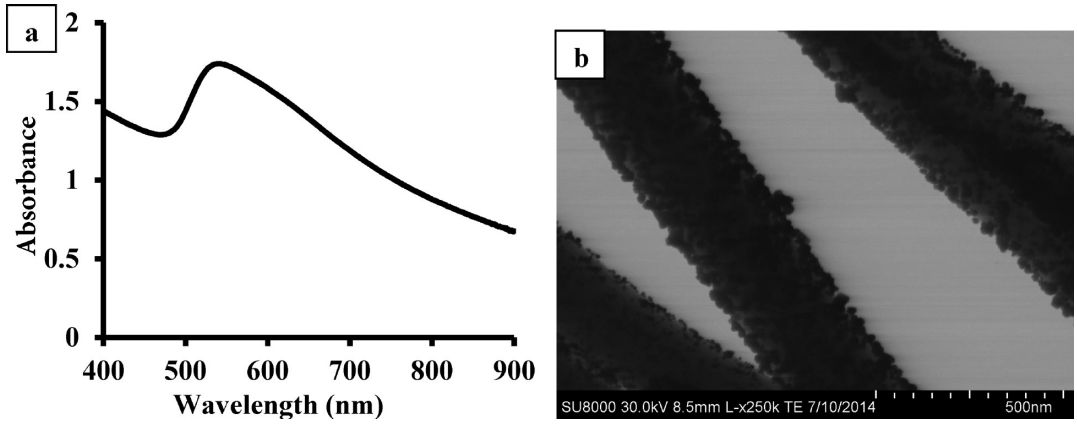

Figure 5. UV−vis spectra (a) and STEM image (b) of Au-SiNW nanohybrids.

dx.doi.org/10.1021/la5020434 | *Langmuir* 2014, 30, 9514−9523

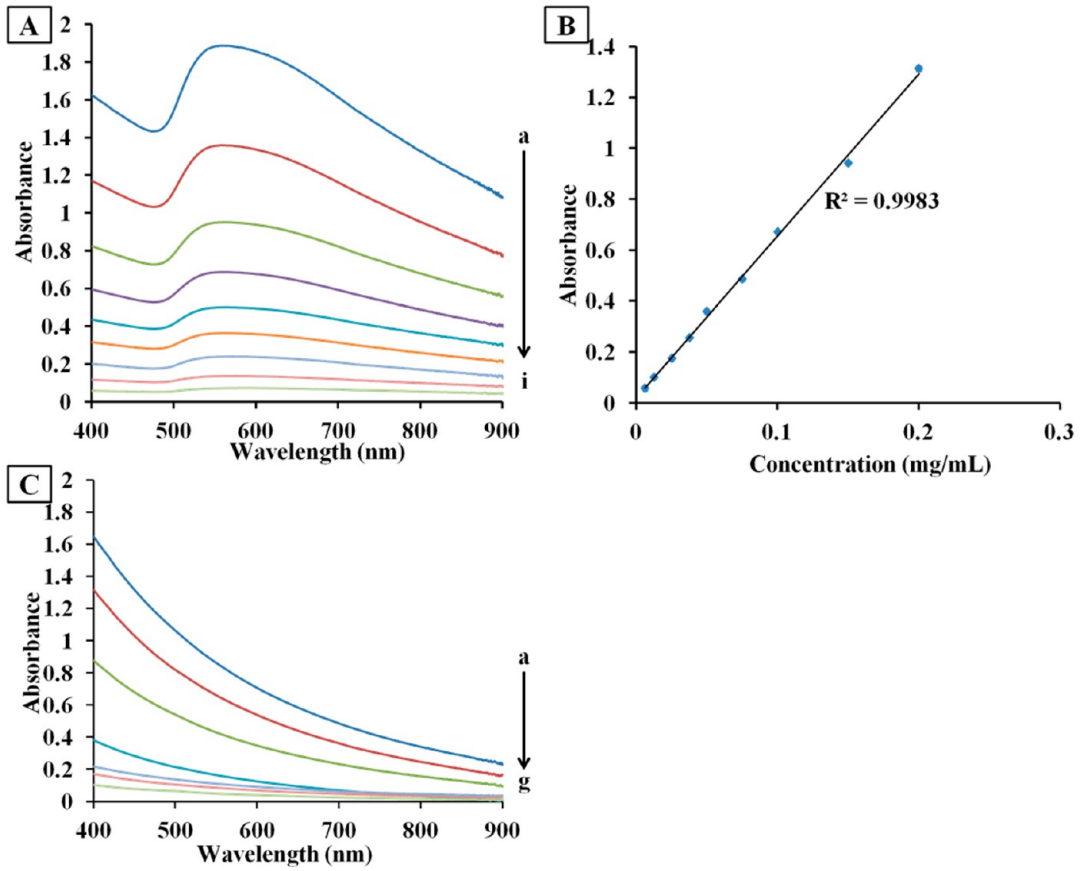

Figure 6. (A) UV−vis spectra of Au-SiNW nanohybrids at different concentrations varying from 0.200, 0.150, 0.100, 0.0750, 0.0500, 0.0375, 0.0250, 0.0125, to 0.00625 mg/mL (a−i). (B) Linear relationship between concentration of Au-SiNW nanohybrids and its absorbance at 808 nm. (C) UV−vis spectra of different concentrations of pure SiNWs changing from 1.00, 0.800, 0.500, 0.250, 0.125, 0.100, to 0.0625 mg/mL (a−g).

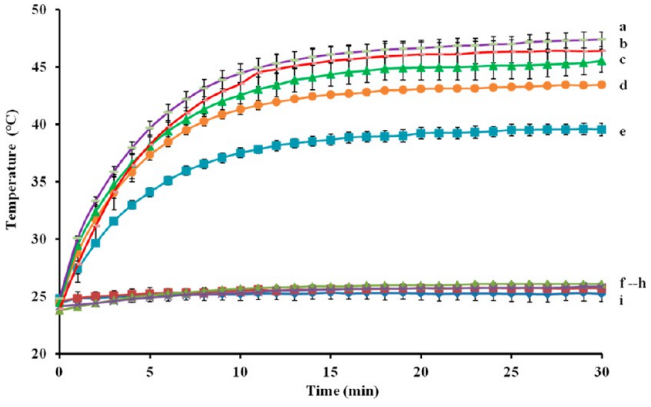

Figure 7. Heat releasing of different concentrations of Au-SiNW nanohybrids varying from 1.000, 0.500, 0.250, 0.100, to 0.050 mg/mL (a−e). Controls: 1.000 mg/mL of AuNPs (f), 1.000 mg/mL of pure SiNWs (g), pure water (h), and cell medium (i).

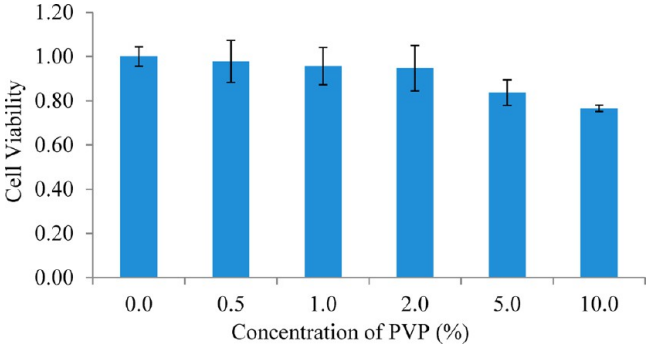

Figure 8. Relative cell viability after culturing A549 cells with different concentrations of PVP varying from 0, 0.5, 1.0, 2.0, 5.0, to 10.0% for 24 h at 37 °C. After the addition of MTT reagent and 4 h incubation at 37 °C, stop solution was added and followed by overnight incubation. The absorbance of each sample was recorded at 560 nm to determine the cell proliferation rate.

iodide (PI), were used in the assay. YO-PRO-1 dye can stain apoptotic cells by penetrating cytoplasm membrane while PI only penetrates nuclear membrane and thus staining necrotic cells. Therefore, the combination of YO-PRO-1 and PI can provide a sensitive indicator for apoptosis detection.

A549 cells were treated with Au-SiNW nanohybrids with different concentrations varying from 0, 0.010, 0.025, 0.050, to 0.100 mg/mL for 2.5 h, followed by irradiating with an 808 nm laser for 20 min. YO-PRO-1 and PI dyes were then added to stain the cells for 10 min. Apoptotic cells showed green fluorescence, whereas necrotic cells showed red fluorescence. As shown in Figure 11a, A549 cells treated by 0.100 mg/mL of Au-SiNW nanohybrids but without the treatment of NIR light irradiation resulted in no necrotic or apoptotic cells detected. By treating A549 cells with both 0.100 mg/mL Au-SiNW nanohybrids and NIR light irradiation, significant apoptosis was induced and stained with the green color (Figure 11b). Although the concentration of Au-SiNW nanohybrids decreased to 0.050 mg/mL, most of the cells were dead after NIR irradiation (Figure 11c). Moreover, green fluorescence was

dx.doi.org/10.1021/la5020434 | *Langmuir* 2014, 30, 9514−9523

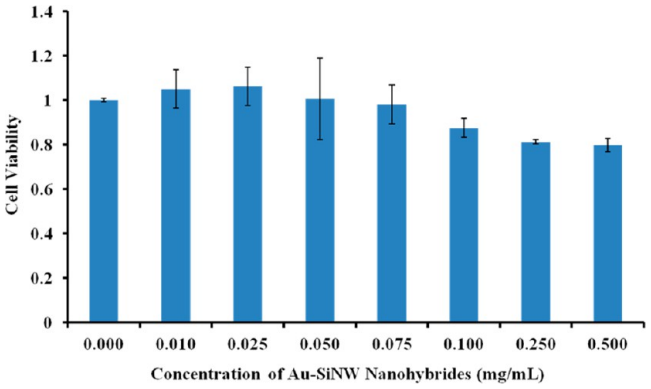

Figure 9. Relative cell viability after culturing with different concentrations of Au-SiNW nanohybrids varying from 0.000, 0.010, 0.025, 0.050, 0.075, 0.100, 0.250, to 0.500 mg/mL for 24 h at 37 °C. After the addition of MTT reagent and 4 h incubation at 37 °C, stop solution was added and followed by overnight incubation. The absorbance of each sample was recorded at 560 nm to determine the cell proliferation rate.

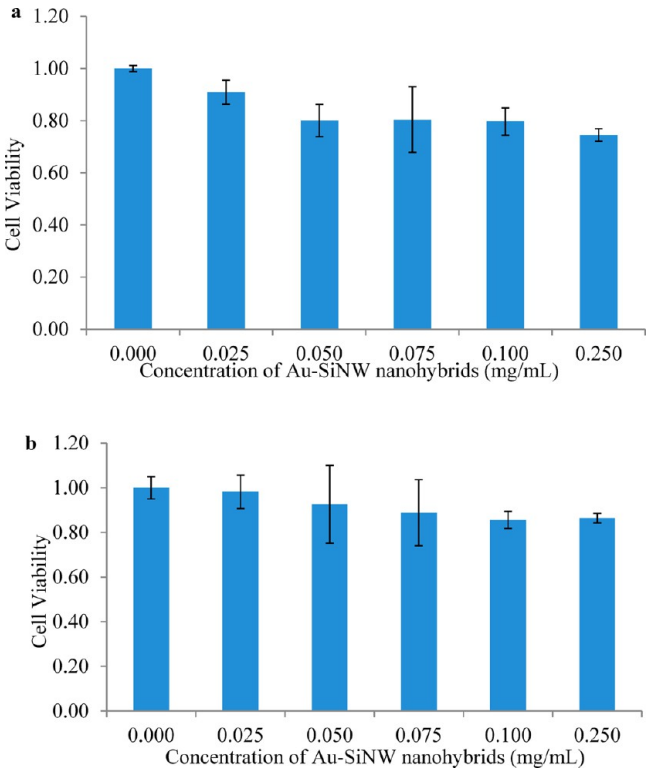

Figure 10. Relative cell viability after culturing with different concentrations of Au-SiNW nanohybrids varying from 0.000, 0.010, 0.025, 0.050, 0.075, 0.100, to 0.250 mg/mL for 24 h at 37 °C. After the addition of MTT reagent and 4 h incubation at 37 °C, stop solution was added and followed by overnight incubation. The absorbance of each sample was recorded at 560 nm to determine the cell proliferation rate. The cells used here were KW12C (a) and SW620 (b).

the dominant color (albeit red color staining for necrotic cells were also observed), indicating that apoptosis was the primary mechanism of cell death. Further decreasing the concentration of Au-SiNW nanohybrids resulted in reduced cell death (Figure 11d,e). These results clearly showed a typical concentration-dependent PTT effect (Figure 11b–e). As a control, no apoptosis or necrotic cells were detected when A549 cells were

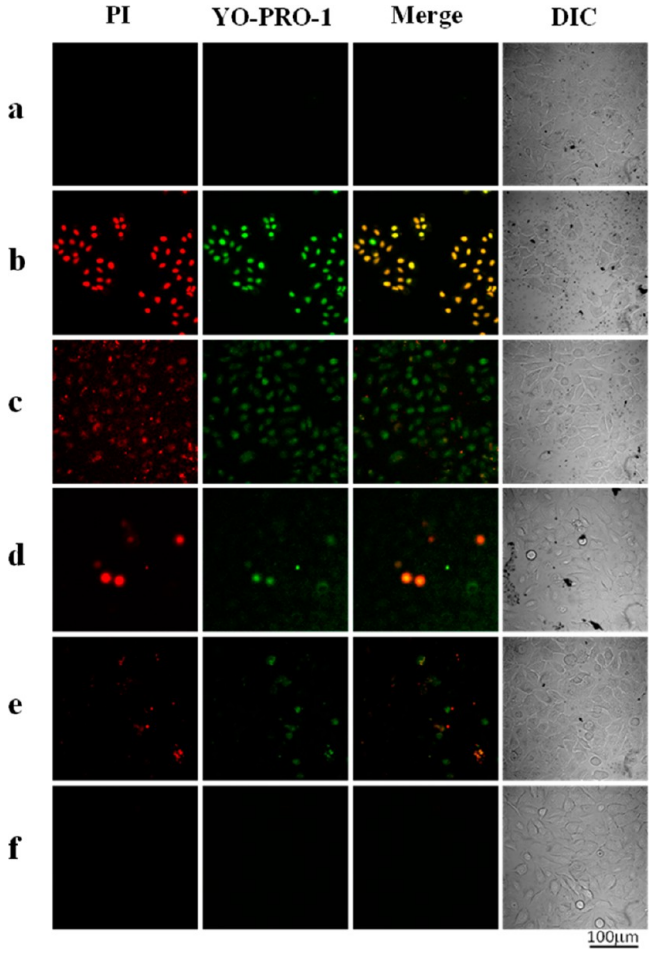

Figure 11. Confocal fluorescence images of A549 cells. A549 cells were treated with different concentrations of Au-SiNW nanohybrids and NIR light centered at 808 nm (0.30 W/cm^2) for 20 min. The concentration of Au-SiNW nanohybrids was 0.100 mg/mL without NIR irradiation (a) and 0.100 (b), 0.050 (c), 0.025 (d), 0.010 (e), and 0.0 mg/mL (f) with NIR irradiation. After staining a cell population, apoptotic cells showed green fluorescence stained by YO-PRO-1, necrotic cells showed red color by PI, and control cells showed little or no fluorescence. DIC = differential interference contrast. Scale bar = 100 μm.

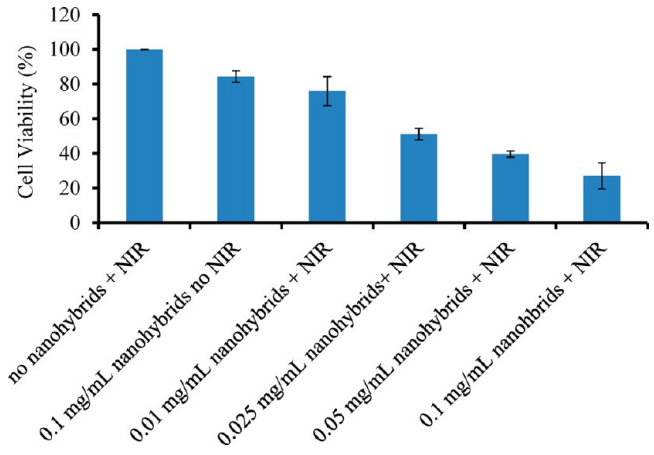

Figure 12. Relative cell viability after incubating with different concentrations of Au-SiNWs nanohybrids in the presence or absence of NIR irradiation.

dx.doi.org/10.1021/la5020434 | *Langmuir* 2014, 30, 9514–9523

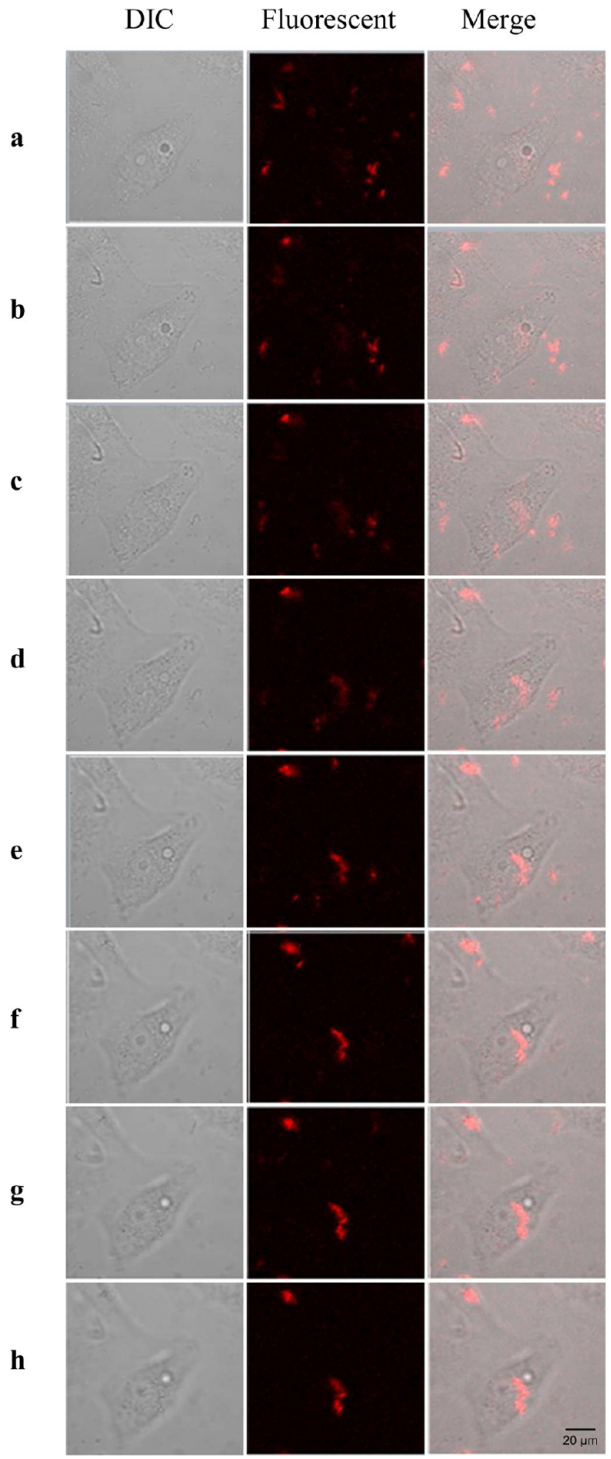

Figure 13. Confocal fluorescence images (*Z*-stack) of A549 cells with the internalization of $Ru(bpy)_3^{2+}$-doped SiNWs. A549 cells were incubated with $Ru(bpy)_3^{2+}$-doped SiNWs for 3 h in 37 °C incubator before taking the images. Images were collected at stacks of 2-D images, occupying the same *x*−*y* position. 0.37 μm intervals with 488 nm laser to create a stack in the *Z*-axis.

only treated by the NIR light in the absence of Au-SiNW nanohybrids (Figure 11f).

MTT experiments were also conducted to quantitatively study the effect of the nanohybrids and NIR irradiation. As shown in Figure 12, with the treatment of NIR irradiation and the increasing concentration from 0.01, 0.025, 0.05, to 0.1 mg/mL, the cell viability decreased to 76.0%, 51.2%, 39.7%, and 27.1%, respectively. However, with the addition of nanohybrids or the treatment of NIR irradiation, no obvious change was observed. These data suggested that only the combination of Au-SiNW nanohybrids and NIR light irradiation can lead to cell death, which was consistent with the results from confocal images.

Considering the relative large size of SiNWs, we also studied the uptake ability of SiNWs by the cancer cells, $Ru(bpy)_3^{2+}$ was chosen to be doped in the matrix of SiNWs and the emitted fluorescence from $Ru(bpy)_3^{2+}$-doped SiNWs can trace the location of the nanohybrids when incubated with A549 cells. A series of *Z*-stack confocal fluorescence images (Figure 13) showed strong fluorescence intensity, indicating the successful uptake of the $Ru(bpy)_3^{2+}$-doped SiNWs by the cells.

4. CONCLUSIONS

In summary, a novel nanomaterial—Au-SiNW nanohybrid—was synthesized with controllable sizes of AuNPs on the surface. This new nanocomposite exhibited strong surface plasmon resonance absorption due to the growth of a gold layer on the surface of SiNWs. The absorption of Au-SiNW nanohybrids can be tuned from the visible to the NIR region simply by changing the amount of $HAuCl_4$ in the gold growth solution. This nanocomposite was found to have excellent biocompatibility. Combining the intrinsic properties of both SiNWs and gold layer, the nanocomposites showed significantly improved photothermal cell destroying efficacy even at a low laser power density of 0.3 W/cm^2. These findings indicate that the nanocomposite may be a promising candidate for phototherapeutic cancer therapy.

AUTHOR INFORMATION

Corresponding Authors

*Ph 701-777-3610; Fax 701-777-2331; e-mail jzhao@chem.und.edu (J.X.Z.).

*Ph 701-777-3610; Fax 701-777-2331; e-mail min.wu@med.und.edu (M.W.).

Notes

The authors declare no competing financial interest.

ACKNOWLEDGMENTS

The work was supported by the National Science Foundation CHE0947043 and NSF CHE 911472 to Julia Xiaojun Zhao and Flight Attendant Medical Research Institute (FAMRI, Grant #103007), NIH AI101973-01, and AI097532-01A1 to Min Wu.

REFERENCES

(1) Kim, J.-H.; Bryan, W. W.; Randall Lee, T. Preparation, Characterization, and Optical Properties of Gold, Silver, and Gold-Silver Alloy Nanoshells Having Silica Cores. *Langmuir* **2008**, *24*, 11147−11152.

(2) Graf, C.; van Blaaderen, A. Metallodielectric Colloidal Core-Shell Particles for Photonic Applications. *Langmuir* **2002**, *18*, 524−534.

(3) Jain, P. K.; El-Sayed, M. A. Surface Plasmon Resonance Sensitivity of Metal Nanostructures: Physical Basis and Universal Scaling in Metal Nanoshells. *J. Phys. Chem. C* **2007**, *111*, 17451−17454.

(4) Wang, H.; Tam, F.; Grady, N. K.; Halas, N. J. Cu Nanoshells: Effects of Interband Transitions on the Nanoparticle Plasmon Resonance. *J. Phys. Chem. B* **2005**, *109*, 18218−18222.

(5) Loo, C.; Lowery, A.; Halas, N.; West, J.; Drezek, R. Immunotargeted Nanoshells for Integrated Cancer Imaging and Therapy. *Nano Lett.* **2005**, *5*, 709−711.

(6) Oldenburg, S. J.; Jackson, J. B.; Westcott, S. L.; Halas, N. J. Infrared Extinction Properties of Gold Nanoshells. *Appl. Phys. Lett.* **1999**, *75*, 2897−2899.
(7) Chen, W. R.; Adams, R. L.; Carubelli, R.; Nordquist, R. E. Laser-Photosensitizer Assisted Immunotherapy: A Novel Modality for Cancer Treatment. *Cancer Lett.* **1997**, *115*, 25−30.
(8) Kam, N. W. S.; O'Connell, M.; Wisdom, J. A.; Dai, H. Carbon Nanotubes as Multifunctional Biological Transporters and Near-Infrared Agents for Selective Cancer Cell Destruction. *Proc. Natl. Acad. Sci. U. S. A.* **2005**, *102*, 11600−11605.
(9) Huang, X.; El-Sayed, I. H.; Qian, W.; El-Sayed, M. A. Cancer Cell Imaging and Photothermal Therapy in the Near-Infrared Region by Using Gold Nanorods. *J. Am. Chem. Soc.* **2006**, *128*, 2115−2120.
(10) Tang, L.; Liu, L. J.; Elwing, H. Complement Activation and Inflammation Triggered by Model Biomaterial Surfaces. *J. Colloid Interface Sci.* **1998**, *41*, 333−340.
(11) Hu, M.; Chen, J.; Li, Z.-Y.; Au, L.; Hartland, G. V.; Li, X.; Marquez, M.; Xia, Y. Gold Nanostructures: Engineering Their Plasmonic Properties for Biomedical Applications. *Chem. Soc. Rev.* **2006**, *35*, 1084−1094.
(12) Shukla, R.; Bansal, V.; Chaudhary, M.; Basu, A.; Bhonde, R. R.; Sastry, M. Biocompatibility of Gold Nanoparticles and Their Endocytotic Fate Inside the Cellular Compartment: A Microscopic Overview. *Langmuir* **2005**, *21*, 10644−10654.
(13) Skrabalak, S. E.; Chen, J.; Au, L.; Lu, X.; Li, X.; Xia, Y. Gold Nanocages for Biomedical Applications. *Adv. Mater.* **2007**, *19*, 3177−3184.
(14) Kim, J.; Park, S.; Lee, J. E.; Jin, S. M.; Lee, J. H.; Lee, I. S.; Yang, I.; Kim, J.-S.; Kim, S. K.; Cho, M.-H.; Hyeon, T. Designed Fabrication of Multifunctional Magnetic Gold Nanoshells and Their Application to Magnetic Resonance Imaging and Photothermal Therapy. *Angew. Chem., Int. Ed.* **2006**, *45*, 7754−7758.
(15) Bartczak, D.; Muskens, O. L.; Nitti, S.; Sanchez-Elsner, T.; Millar, T. M.; Kanaras, A. G. Interactions of Human Endothelial Cells with Gold Nanoparticles of Different Morphologies. *Small* **2012**, *8*, 122−130.
(16) Wang, S. M.; Xiao, J. J.; Yu, K. W. Tunable Coupled Plasmon Modes via Nanoshell Particle Chains. *Opt. Commun.* **2007**, *279*, 384−389.
(17) Gobin, A. M.; O'Neal, D. P.; Watkins, D. M.; Halas, N. J.; Drezek, R. A.; West, J. L. Near Infrared Laser-Tissue Welding Using Nanoshells as an Exogenous Absorber. *Lasers Surg. Med.* **2005**, *37*, 123−129.
(18) Gobin, A. M.; Lee, M. H.; Halas, N. J.; James, W. D.; Drezek, R. A.; West, J. L. Near-Infrared Resonant Nanoshells for Combined Optical Imaging and Photothermal Cancer Therapy. *Nano Lett.* **2007**, *7*, 1929−1934.
(19) Wu, C.; Liang, X.; Jiang, H. Metal Nanoshells as a Contrast Agent in Near-Infrared Diffuse Optical Tomography. *Opt. Commun.* **2005**, *253*, 214−221.
(20) Gelbrich, T.; Feyen, M.; Schmidt, A. M. Magnetic Thermoresponsive Core-Shell Nanoparticles. *Macromolecules* **2006**, *39*, 3469−3472.
(21) Levin, C. S.; Hofmann, C.; Ali, T. A.; Kelly, A. T.; Morosan, E.; Nordlander, P.; Whitmire, K. H.; Halas, N. J. Magnetic-Plasmonic Core-Shell Nanoparticles. *ACS Nano* **2009**, *3*, 1379−1388.
(22) Yang, Y.; Liu, J.; Li, X.; Liu, X.; Yang, Q. Organosilane-Assisted Transformation from Core-Shell to Yolk-Shell Nanocomposites. *Chem. Mater.* **2011**, *23*, 3676−3684.
(23) Zeng, H.; Li, J.; Wang, Z. L.; Liu, J. P.; Sun, S. Bimagnetic Core/Shell FePt/Fe_3O_4 Nanoparticles. *Nano Lett.* **2003**, *4*, 187−190.
(24) Schmit, V. L.; Martoglio, R.; Scott, B.; Strickland, A. D.; Carron, K. T. Lab-on-a-Bubble: Synthesis, Characterization, and Evaluation of Buoyant Gold Nanoparticle-Coated Silica Spheres. *J. Am. Chem. Soc.* **2011**, *134*, 59−62.
(25) Jackson, J. B.; Halas, N. J. Silver Nanoshells: Variations in Morphologies and Optical Properties. *J. Phys. Chem. B* **2001**, *105*, 2743−2746.
(26) Goude, Z. E.; Leung, P. T. Surface Enhanced Raman Scattering from Metallic Nanoshells with Nonlocal Dielectric Response. *Solid State Commun.* **2007**, *143*, 416−420.
(27) Hale, G. D.; Jackson, J. B.; Shmakova, O. E.; Lee, T. R.; Halas, N. J. Enhancing the Active Lifetime of Luminescent Semiconducting Polymers via Doping with Metal Nanoshells. *Appl. Phys. Lett.* **2001**, *78*, 1502−1504.
(28) Xu, S.; Hartvickson, S.; Zhao, J. X. Engineering of SiO_2-Au-SiO_2 Sandwich Nanoaggregates Using a Building Block: Single, Double, and Triple Cores for Enhancement of Near Infrared Fluorescence. *Langmuir* **2008**, *24*, 7492−7499.
(29) Peters, R.; Kramer, E.; Oomen, A. G.; Herrera Rivera, Z. E.; Oegema, G.; Tromp, P. C.; Fokkink, R.; Rietveld, A.; Marvin, H. J. P.; Weigel, S.; Peijnenburg, A. A. C. M.; Bouwmeester, H. Presence of Nano-Sized Silica during *in vitro* Digestion of Foods Containing Silica as a Food Additive. *ACS Nano* **2012**, *6*, 2441−2451.
(30) Farre, C.; Lansalot, M.; Bazzi, R.; Roux, S. p.; Marquette, C. A.; Catanante, G. l.; Blum, L. c. J.; Charvet, N.; Louis, C. d.; Chaix, C. Automated Oligonucleotide Solid-Phase Synthesis on Nanosized Silica Particles Using Nano-on-Micro Assembled Particle Supports. *Langmuir* **2009**, *26*, 4941−4950.
(31) Fujiwara, M.; Shiokawa, K.; Sakakura, I.; Nakahara, Y. Silica Hollow Spheres with Nanomacroholes like Diatomaceous Earth. *Nano Lett.* **2006**, *6*, 2925−2928.
(32) Zhang, Y.; Li, G.; Wu, Y.; Luo, Y.; Zhang, L. The Formation of Mesoporous TiO_2 Spheres *via* a Facile Chemical Process. *J. Phys. Chem. B* **2005**, *109*, 5478−5481.
(33) Hahn, M.; Singh, A.; Sharma, P.; Brown, S.; Moudgil, B. Nanoparticles as Contrast Agents for *in vivo* Bioimaging: Current Status and Future Perspectives. *Anal. Bioanal. Chem.* **2011**, *399*, 3−27.
(34) Kennedy, L. C.; Bickford, L. R.; Lewinski, N. A.; Coughlin, A. J.; Hu, Y.; Day, E. S.; West, J. L.; Drezek, R. A. A New Era for Cancer Treatment: Gold-Nanoparticle-Mediated Thermal Therapies. *Small* **2011**, *7*, 169−183.
(35) Tong, L.; Wei, Q.; Wei, A.; Cheng, J.-X. Gold Nanorods as Contrast Agents for Biological Imaging: Optical Properties, Surface Conjugation and Photothermal Effects. *Photochem. Photobiol.* **2009**, *85*, 21−32.
(36) Au, L.; Zheng, D.; Zhou, F.; Li, Z.-Y.; Li, X.; Xia, Y. A Quantitative Study on the Photothermal Effect of Immuno Gold Nanocages Targeted to Breast Cancer Cells. *ACS Nano* **2008**, *2*, 1645−1652.
(37) ANSI, American National Standard for Safe Use of Lasers, Laser Institute of America, Orlando, FL, 2000.
(38) Park, S.; Heo, J.; Kim, H. J. A Noval Route to the Synthesis of Silica Nanowires without a Metal Catalyst at Room Temperature by Chemical Vapor Deposition. *Nano Lett.* **2011**, *11*, 740−745.
(39) Yang, Z.; Zhang, Y.; Liu, D.; Nie, E.; Jiao, Z.; Jin, Y.; He, Y.; Gong, M.; Sun, X. Selective Synthesis of SiO_2 NWs on Si Substrate and Their Adjustable Photoluminescence. *J. Non-Cryst. Solids* **2010**, *356*, 2207−2210.
(40) Ramgir, N. S.; Sekhar, P. K.; Zajac, A.; Lee, L.; Zhukov, T.; Bhansali, S. Ultrasensitive Voltammetric Detection of IL-10, a Lung Cancer Biomarker, in Serum Using SiO_2 Nanowires Template. *Sens. Lett.* **2007**, *5*, 608−611.
(41) Elliman, R. G.; Wilkinson, A. R.; Kim, T. H.; Sekhar, P. K.; Bhansali, S. Optical Emission from Erbium-Doped Silica Nanowires. *J. Appl. Phys.* **2008**, *103*, 104304−104309.
(42) Ramgir, N. S.; Zajac, A.; Sekhar, P. K.; Lee, L.; Zhukov, T. A.; Bhansali, S. Voltammetric Detection of Cancer Biomarkers Exemplified by Interleukin-10 and Osteopontin with Silica Nanowires. *J. Phys. Chem. C* **2007**, *111*, 13981−13987.
(43) Hermanson, G. T., Ed.; *In Bioconjugate Techniques*; Academic Press: San Diego, 1996; p 597.
(44) Wu, M.; Pasula, R.; Smith, P. A.; Martin, W. J., II Mapping Alveolar Epithelial Binding Sites in Vivo Using Phase Peptide Libraries. *Gene Ther.* **2003**, *10*, 1429−1436.
(45) Kannan, S.; Pang, H.; Foster, D.; Rao, Z.; Wu, M. Human 8-oxoguanine DNA Glycosylase Links MAPK Activation to Resistance

to Hyperoxia in Lung Epithelial Cells. *Cell Death Differ.* **2006**, *13*, 311−323.
(46) Graf, C.; Vossen, D. L. J.; Imhof, A.; van Blaaderen, A. A General MEthod to Coat Colloidal Particles with Silica. *Langmuir* **2003**, *19*, 6693−6700.
(47) Pattanaik, M.; Bhaumik, S. K. Adsorption Behavior of Polyvinyl Pyrrolidone on Oxide Surfaces. *Mater. Lett.* **2000**, *44*, 352−360.
(48) Duff, D. G.; Baiker, A.; Edwards, P. P. A New Hydrosol of Gold Cluster. 1. Formation and Particle Size Variation. *Langmuir* **1993**, *9*, 2301−2309.
(49) Oh, W.-K.; Kim, S.; Choi, M.; Kim, C.; Jeong, Y. S.; Cho, B.-R.; Hahn, J.-S.; Jang, J. Cellular Uptake, Cytotoxicity, and Innate Immune Response of Silica-Titania Hollow Nanoparticle Based on Size and Surface Functionality. *ACS Nano* **2010**, *4*, 5301−5313.